Published in final edited form as:
Nanoscale. 2013 October 21; 5(20): 9839–9847. doi:10.1039/c3nr03205a.

Sulfidation of silver nanowires inside human alveolar epithelial cells: a potential detoxification mechanism

Shu Chen[1], **Angela E. Goode**[1], **Sinbad Sweeney**[2], **Ioannis G. Theodorou**[1], **Andrew J. Thorley**[2], **Pakatip Ruenraroengsak**[1,2], **Yan Chang**[3], **Andrew Gow**[4], **Stephan Schwander**[5], **Jeremy Skepper**[6], **Junfeng (Jim) Zhang**[3], **Milo S. Shaffer**[7], **Kian Fan Chung**[2], **Teresa D. Tetley**[2], **Mary P. Ryan**[1], and **Alexandra E. Porter**[1,*]

[1]Department of Materials and London Centre for Nanotechnology, Imperial College London, Exhibition Road, London SW7 2AZ, UK

[2]National Heart and Lung Institute, Imperial College London, UK

[3]Department of Preventive Medicine, Keck School of Medicine, University of Southern California, USA

[4]Department of Pharmacology and Toxicology at Rutgers University, Piscataway, NJ, USA

[5]Department of Environmental and Occupational Health, University of Medicine and Dentistry (UMDNJ) School of Public Health, New Jersey, USA

[6]Multi-Imaging Centre, Department of Physiology, Development and Neuroscience, University of Cambridge, Downing Street, Cambridge CB2 3DY, UK

[7]Department of Chemistry and London Centre for Nanotechnology, Imperial College London, Exhibition Road, London SW7 2AZ, UK

Keywords

Silver Nanowires (AgNWs); silver sulfidation, silver sulfide (Ag_2S); dissolution; toxicity

Introduction

The respiratory system is potentially an important route of exposure to nano-Ag during their synthesis, use and disposal. Inhaled Ag nanomaterials have the potential to generate significant biological consequences within, and beyond, the respiratory tract as they are likely to be deposited into the deep alveolar region. Here the epithelial-endothelial gas-blood barrier is very thin (< 0.5 μm), consisting of a monolayer of type I or type II epithelial cells which share a basement membrane with the underlying capillary endothelium to facilitate gas exchange.[1] Any cellular or protein damage in this region could impact on pulmonary homeostasis and possibly compromise gas exchange. It is important therefore to understand

*Corresponding author: a.porter@imperal.ac.uk.

Supporting Information Available: ICSD information of silver and various silver compounds, SAED of as-synthesized AgNWs, STEM-EDX spectra collected from areas 4–6 in Figure 3e and g, characterization of AgNWs chemistry and morphology change in ambient air, and the effect of the osmium staining and the embedding procedure on AgNWs stability are provided.

the interactions of Ag nanomaterials at this interface in order to anticipate their adverse effects and manage the risk of their toxicological effects.

Recent evidence shows that *in vitro* exposure to spherical, or near spherical, silver nanoparticles (AgNPs) leads to oxidative stress, lipid peroxidation, inhibition of mitochondrial activity, DNA damage and apoptotic cell death suggested to be due to the release of Ag^+ ions.[2–13] The interaction of Ag^+ with thiol groups of proteins may cause interruption of normal cell events by inhibiting their activity, whilst Ag^+ might perturb mitochondrial function through interactions with thiol groups within the mitochondrial inner membrane, causing oxidative damage.[14–16] However, results from published studies concerning the toxicity of Ag nanomaterials are frequently inconclusive, with studies suggesting that AgNP toxicity can be linked to Ag^+ ion release[13, 17] or from a contribution of both Ag^+ ion release and particle effects.[18–21]

A number of studies indicate that the transformation of AgNPs to highly insoluble Ag_2S NPs reduces the potential adverse environmental effects of silver[22–26] Furthermore, it was reported that the degree of Ag transformation to Ag_2S controlled by pre-aging AgNPs with the hydrosulfide anion (HS^-), correlates with the ability of AgNPs to inhibit *E.Coli* growth which decreases as the Ag_2S:Ag^0 ratio of the sulfidized NPs increases.[27] However, it is not known whether a similar process of Ag sulfidation occurs in the lung. Sulfide species, including hydrogen sulfide gas (H_2S), HS^- and sulfide (S^{2-}), exist in all human tissues, including the lung. H_2S is an important gasomediator resulting from tissue de-sulfhydration of cysteine and is rapidly broken down by a combination of chemical and enzyme reactions. The free gas H_2S level in tissue is likely to be maintained on the order of nM concentrations; however, the total concentration of sulfide species is thought to be much higher (~ μM).[12, 28, 29] Thus, it is hypothesized that the interaction of AgNPs with pulmonary sulfur species could be an important detoxification mechanism in the lung. The fact that most of the toxicity studies performed on AgNPs so far have overlooked their possible sulfidation, might be one of the reasons leading to inconsistent results.

Shape and size are important factors in determining uptake mechanisms and the long term ramifications of nanomaterial exposure. Fibrous nanomaterials, such as nanotubes and nanowires have been studied with respect to their uptake mechanisms and the onset of frustrated macrophage phagocytosis has been stated as an important factor in the post-exposure inflammatory response. In particular comparisons with asbestos fibres in the lung, and induced mesothelioma, have been made to multi-walled carbon nanotubes with high aspect ratios.[30] Recent *in vivo* work has shown frustrated macrophage uptake of silver nanowires (AgNWs) that are greater than 10 μm in length.[31] Whilst that work was able to show AgNWs within membrane bound vesicles as well as in the pleural space, the technique used (and its limited resolution) did not allow any quantitative analysis of dissolution or changes to the AgNW chemistry to structure after cellular uptake.

In this study, we have investigated the transformation of AgNWs in relation to cell viability and oxidative stress, during and following uptake by transformed human alveolar type 1 epithelial cells (TT1),[32] which account for over 95% of the alveolar surface and are a major target of inhaled nano-sized objects. In order to do this, we have used a combination of high

resolution and analytical transmission electron microscopy (TEM) to monitor the interaction of AgNWs with TT1 cells over time. We have avoided the oxidative effects of heavy metal staining techniques,[10,21] which may accelerate dissolution or oxidation of the nanostructures and thus change the observed morphologies. Furthermore, our recent unpublished research suggests that it is important to exclude any extracellular transformation of AgNWs or chemical interactions that might occur in the tissue culture exposure medium as these might modify the subsequent intracellular processes. It is therefore vital to characterise the physicochemical properties of the AgNWs *at the point of cell exposure* in order to draw accurate conclusions linking the physicochemical properties of the AgNWs to their bioreactivity. A combination of high angle annular dark field (HAADF) scanning transmission electron microscopy (STEM), a technique which is highly sensitive to local variations in the atomic number within a sample, and energy-dispersive X-ray spectroscopy (EDX) was used to define the subcellular localisation and the morphological and chemical features of individual AgNWs within TT1 cells. Electron microscopy results were correlated with any changes in cell viability and induction of oxidative stress over time.

Pure AgNWs were synthesized through a modified polyol pathway through the reduction of $AgNO_3$ with ethylene glycol in the presence of poly(vinyl pyrrolidone) (PVP).[33] The AgNWs were purified to remove excess free Ag^+ ions which may contribute to their toxicity.[34] The as-synthesized AgNWs have a negative surface charge of −14.8 ± 0.1 mV in DI-H_2O. The concentration of free Ag^+ ions in as-synthesised AgNWs DI-H_2O solution is below the ICP-OES detection limit (i.e. < 1 ppb).

The crystalline structure and composition of as-synthesised AgNWs was confirmed by TEM and EDX spectra prior to cell exposure. The AgNWs were 72 ± 36 nm in diameter and 1.5 ± 1.4 μm long (Figure 1a-c); they had a lattice spacing of 0.24 nm, consistent with the (111) interplanar spacing of bulk Ag (ref 01-087-0597, Supplementary, Table S1) (Figure 1e). The interplanar spacings extracted from the selected area electron diffraction (SAED) patterns (Supplementary, Figure S1) were also consistent with metallic Ag (ref 01-087-0597). A representative EDX spectrum showing only peaks corresponding to Ag, collected from one AgNW, is shown in Figure 1f.

To examine the distribution of AgNWs inside TT1 cells as a function of exposure time, the TT1 cells were pulsed with AgNWs for one hour in RPMI cell culture medium, then washed, cultured for a further hour in RPMI, washed and cultured for up to 7 days in DCCM-1 medium. The use of RPMI ensured that the AgNWs did not dissolve or transform to Ag_2S in the cell culture medium before any interactions with TT1 cells. In order to maintain normal cell activity, DCCM-1, a cell medium which provides nutrition for cells was used for further incubation after Ag exposure.[32] Figure 2a shows an AgNW translocating across the plasma membrane. This “needle-like” mechanism of insertion into cells has been reported previously for functionalized carbon nanotubes.[35] After a 1 h pulse, AgNWs were found within endosome-like vesicles, and also frequently within the cytoplasm of the cells (Figure 2b-c). 24 hours after the exposure pulse, internalized AgNWs were observed within the cytoplasm and within endosome- and lysosome-like vesicles (Figure 2d-f). 7 days following the exposure pulse, the distribution of the AgNWs was similar to that found in the 24 hour exposed cells (Figure 2g-i).

Having studied the internalisation and distribution of AgNWs in the TT1 cells, we proceeded to investigate the intracellular changes in morphology and chemistry of these AgNWs over time. Further STEM images and EDX spectra were taken after an AgNW exposure pulse of 1 hour and a chase in fresh medium of 24 hours and 7 days (Figure 3). No heavy metal staining process was used in order to preserve the morphology and chemistry of AgNWs (supplementary, Figure S3). Again, precautions were taken to avoid AgNW sulfidation in the ambient air, the cell culture medium or during processing for TEM imaging and analysis (supplementary, Figure S4 and S5).

Effect of one hour exposure

After a 1 h pulse, small particles (3–9 nm diameter) were observed surrounding the ends of the AgNWs (Figure 3b). Ag (L) peaks and S (K) peaks were detected in STEM-EDX spectra of these small particles (Figure 3c, spectrum 1), whereas the bulk of the AgNWs was pure Ag (Figure 3c, spectrum 2). The shape of the AgNWs was retained, although there was a reduction in the contrast at the ends of the wire, where the particles were located (Figure 3b). Diffuse Ag was observed near to the longitudinal edge of the AgNWs indicative of dissolution processes (Figure 3b, insert). The presence of Ag was confirmed by the STEM-EDX spectrum at the observed dissolution sites (Figure 3c, spectrum 3). This asymmetric behaviour, *i.e.* greater reactivity at the tip of the AgNW, was expected, as this surface is close-packed, has high surface energy, will contain a higher density of surface defects than the bulk or longitudinal edges of the wire and hence will be more susceptible to dissolution (Figure 3b).

Effect after 24 hours and 7 days post-exposure pulse

Dissolution and sulfidation of the AgNWs was more substantial after 24 h and 7 days post-exposure (Figure 3d-i), as indicated by greater roughening of the AgNW surface and the presence of a larger number of particles surrounding the AgNWs (Figure 3e and g). Variations in the S:Ag ratio between the tip, surface and particles surrounding the AgNWs after 1 hour exposure and 24 hours and 7 days post-exposure are summarised in Table 1 (the EDX spectra taken from each position are provided in supplementary, Figure S2.

24 hours post-exposure

As indicated in Figure 3, at 24 hours post-exposure, the most substantial release of diffuse Ag was again observed at the of the wire (Figure 3e). The nonstoichiometric S/Ag ratio of 1.15 (Table 1) was higher than the EDX S/Ag ratio of 0.44 for in house synthesized Ag_2S NPs.[36, 37] The higher ratio observed in the current study suggests either a high association of Ag^+ ions with intracellular S-containing compounds or proteins, and/or a rapid chemisorption of excess S, before formation of Ag_2S.[22]

7 days post-exposure

After 7 days, the intracellular AgNWs had dissolved more extensively. Compared to the 1 h and 24 h study times, a larger number of particles surrounded the AgNWs (Figure 3g). Particles had coalesced with each other to form a shell coating the AgNW. Particles had a

lattice spacing of 0.29 nm, close to the monoclinic structure of Ag_2S (−112) (ref 00-014-0072) (Figure. 3h). SAED further confirmed that these particles were crystalline Ag_2S (Figure 3i). The interplanar spacings measured from the SAED patterns were consistent with bulk monoclinic Ag_2S (ref 00-014-0072, supplementary, Table S1). The EDX spectrum taken from the particles surrounding the AgNWs (Table 1) indicates the existence of Ag_2S. 95 % of the AgNWs had sulfidised after 1 h exposure to AgNWs and 100 % of Ag NWs had sulfidized for 24 h and 7 days samples (n=80, for each time point). Taken together, our observations indicate that intracellular internalisation of AgNWs results in dissolution of the AgNWs and precipitation of highly insoluble Ag_2S (K_{sp}=5.92•10^{-51}) which occurs even during the 1 hour exposure period, becoming more extensive over the 7 days post-exposure.

Effect of AgNWs on TT1 cell viability and generation of reactive oxygen species (ROS)

In this study, we were particularly focussed on AgNWs uptake by TT1 cells as another mechanism of translocation, and in particular to discern AgNWs bioreactivity and/or cytotoxicity. AgNWs were detected inside TT1 cells, where they had degraded through an Ag to Ag_2S transformation process. The impact of this transformation of AgNWs in relation to cell viability and oxidative stress, during and following uptake by TT1 cells was further investigated. The 1 hour exposure of TT1 cells to AgNWs had no significant effect on cell viability (*$p < 0.05$, **$p < 0.01$) at any time interval, even up to 24 h post exposure (Figure 4c). In addition, the generation of ROS in TT1 cells exposed to AgNWs was investigated using the oxidative stress fluorescent marker, dihydroethidium (DHE), which is a cell permeable fluorescent dye which can be oxidized by ROS, and produces a detectable red fluorescent signal. There was no ROS generation as indicated by the absence of a red fluorescence signal (Figure 4d), which correlated well with the cell viability results. Thus, AgNWs exerted no TT1 cell toxicity; we suggest that this is likely due to low level of free Ag^+ ions which become trapped as insoluble Ag_2S as they encounter cellular sulfur species.

A schematic drawing of AgNWs travel into the deep lung (alveolar region) and a proposed sulfidation mechanism of AgNWs inside type I epithelia cells are presented in Figure 5. Like other thin materials (with diameters ≤ 1 μm), AgNWs are respirable and can travel deep inside the lung and deposit beyond the ciliated airways,[31, 38] into the alveolar region where gas exchange takes place (Figure 5a). The alveolar epithelium is comprised of a monolayer of alveolar type I and alveolar type II epithelial cells, covered by a layer of pulmonary surfactant produced by type II cells. Where the attenuated type I cells abut the underlying capillary endothelial cells, the gas-blood barrier is very thin (< 0.5 μm) and therefore allows gas exchange and transfer of solutes across this interface (Figure 5b).[1] Clearance of particles deposited inside the alveoli relies mostly on alveolar macrophage phagocytosis; macrophages migrate out of the alveolar region and are subsequently cleared out of the lung via the mucociliary escalator. It is suggested that alveolar macrophages are most efficient at phagocytosing particles in the 1–3 μm range[39]; particles that exceed the maximal length of a macrophage (15–20 μm), and hence avoid phagocytosis, can lead to unsuccessful removal of the materials by macrophages, activation of macrophages and inflammation, as is the case

for asbestos fibres. [40, 41] Particles that are not phagocytosed by macrophages, due to their extreme length, macrophage overload and death, or even due to their small size, will interact with the epithelial cells,[38, 42] especially type I cells which cover 95 % of the alveolar surface. The interaction of cell free particles with epithelial cells is suggested to contribute to subsequent pathologies, such as asbestosis,[40] and lead to epithelial cell necrosis or apoptosis, release of pro-inflammatory cytokines and might even compromise the integrity of the epithelium and increase the chance of transferring nanomaterials across the air-blood barrier to the interstitium and systemic circulation.[43]

However, in contrast to other biopersistant materials, *e.g.* asbestos, our results revealed that AgNWs can be degraded within the cellular environment and transform to Ag_2S. This significantly limits the short term toxicity of AgNWs and their impact on human physiology. The cellular sulfidation of the AgNWs may occur via two chemical reactions:

1. Oxidative/precipitation (an in-direct) pathway, *i.e.* oxidative dissolution of silver (reaction eq. 1a) followed by sulfide precipitation (reaction eq.1b–d). This sulfidation process is effectively independent of sulfide concentration, due to the extremely low $K_{sp}$of Ag_2S, but determined by the oxidative dissolution rate of silver. [24]

$$2Ag+\frac{1}{2}O_2+2H^+ \rightarrow 2Ag^+ + H_2O \quad (1a)$$

$$2Ag^+ + H_2S \rightarrow Ag_2S + 2H^+ \quad (1b)$$

$$2Ag^+ + HS^- \rightarrow Ag_2S + H^+ \quad (1c)$$

$$2Ag^+ + S^{2-} \rightarrow Ag_2S \quad (1d)$$

2. particle-fluid reaction, *i.e.* a direct oxysulfidation route (reaction eq. 2a–c), which is dependent on the sulfide concentration, such that the reaction rate increases as the sulfide concentration increases.

$$4Ag+O_2+2H_2S \rightarrow 2Ag_2S+2H_2O \quad (2a)$$

$$4Ag+O_2+2HS^- \rightarrow 2Ag_2S+2OH^- \quad (2b)$$

$$4Ag+O_2+4H^++2S^{2-} \rightarrow 2Ag_2S+2H_2O \quad (2c)$$

As suggested by our TEM study, the sulfidation transformation process is likely dominated by the in-direct pathway at the early stage. The Ag^+ ions dissolve from the AgNWs surface and diffuse into the cellular environment; Ag^+ ions are rapidly re-precipitated as Ag_2S nanoparticles within the comparatively S-rich cytoplasm (Figure 5C-1). With time, more

Ag^+ ions dissolve, migrate within the microenvironment of the AgNWs, and precipitate as new Ag_2S nanoparticles or grow on the existing Ag_2S nuclei. On the other hand, S-species also attack the AgNWs surface through the direct oxylsulfidatoin reaction, a relatively slower reaction as observed in this study, lead to formation of small Ag_2S nanoparticles around the AgNWs surface (Figure 5C-2). These small particles on the surface then act as nuclei, to grow bigger Ag_2S particles and coalescence to form a shell-like structure, which may slow the dissolution rate of Ag^+ ions (Figure 5C-3).

In conclusion, we provide compelling evidence that Ag^+ is released from AgNWs inside epithelial cells and that the Ag^+ ions precipitate as Ag_2S. We suggest that this process occurs by the action of sulfide species including H_2S, HS^- and S^{2-} inside the cells. This process is thermodynamically preferred due to the extremely low solubility of Ag_2S (K_{sp}=5.92•10^{-51}) as compared to other Ag species, such as silver chloride (K_{sp} =1.77•10^{-10}) or silver oxide (K_{sp} =4•10^{-}).[15,27] Although the dissolved Ag^+ ions diffuse within the microenvironment of the AgNWs, they are rapidly re-precipitated as Ag_2S nanoparticles within the comparatively S-rich cytoplasm. In addition, Ag_2S particle formation was observed to take place at the surface of AgNWs. These Ag_2S particles continue to grow and finally coalesce with each other to form an Ag_2S shell, which coats the AgNWs. We postulate that Ag_2S formation limits cell death from ROS production, which might otherwise be expected to occur in the presence of free Ag^+. We further suggest that formation of Ag_2S acts as a Ag^+ ion 'trap' that will significantly limit the short-term toxicity of nano-Ag and their impact on human physiology; similar to suggestions about the trapping of Ag^+ ions by environmental sulfur.[12] These findings have important implications for predicting the long term effects of other classes of Ag nanostructures (AgNPs and plates) which may be dominated by the thermodynamic stability of the Ag_2S and the strong oxidative capability of Ag on S-rich proteins. Furthermore, our study provides insights into the mechanism of degradation of AgNWs *in vivo*, through a sulfidation process which transfroms Ag into Ag_2S. This sulfiation is likely to occur due to the abundance of sulfide species in all human tissues, including hydrogen sulfide gas (H_2S), the hydrosulfide anion (HS^-) and sulfide (S^{2-}). This new insight into the mechanisms by which Ag nanostructures react in cells, suggests that the toxicity of Ag nanomaterials present in consumer products should be considered in the light of these observations, since their *in vivo* reactivity will change significantly over their lifetime, and will depend on which body compartment they target, the nature of the extracellular fluid, and cellular uptake processes.

Methods

AgNW synthesis

Ethylene Glycol (EG, Sigma-Aldrich, anhydrous, 99.8%; 5.5 mL) was placed in a double-neck round-bottom flask connected to a condenser. A stock solution of 0.05 M Sodium chloride (NaCl) was prepared by dissolving NaCl in EG by sonication. The appropriate amount of NaCl stock solution was added to the flask so that the concentration of NaCl in the final reaction volume was 60 μM. The flask was heated in an oil bath at 160°C, to remove trace amounts of water. Meanwhile, argon flow and magnetic stirring were applied and maintained throughout the synthesis. Silver Nitrate ($AgNO_3$, 25 mM, Sigma-Aldrich,

>99%,) and poly(vinyl pyrrolidone) (PVP, Sigma-Aldrich), with an average molecular weight Mw≈360k, were dissolved in 3.5 mL EG by magnetic stirring in the dark. The molar ratio of PVP to $AgNO_3$ was 1.5, where the concentrations of PVP were calculated in terms of the repeating unit. After 1 hour of heating of the reaction flask, 3 mL of the $AgNO_3$/PVP/EG solution were added drop-wise. After injection, the reaction mixture was refluxed at 160 °C and went through a number of colour changes until the mixture became stable at approximately 90 min. The reaction was quenched by cooling the flask in a room-temperature water bath. The reaction mixture was transferred to a centrifuge tube and diluted with acetone 5 times by volume. The AgNWs were collected by centrifugation at 4500 rpm for 10 min. The washing process was repeated with ethanol and deionized water, to ensure that most of the EG and PVP were removed. The sample was finally dispersed in 5 mL of deionised water.[33]

Particle exposure and viability assays

MTS is a novel tetrazolium compound, 3-(4,5-dimethylthiazol-2-yl)-5-(3-carboxymethoxyphenyl)-2-(4-sulfophenyl)-2H-tetrazolium, that can be reduced by dehydrogenase enzymes within living cells demonstrating cellular metabolic activity and cell viability. Such reduction in the presence of an electron coupling reagent, phenazine ethosulfate (MPS), results in the production of formazan product that is soluble in tissue culture medium and the absorbance of this formazan product can be measured using spectrophotometer. Cells were seeded on 96-well plates at density of 10,000 cells/well in complete medium (containing 10% NCS, 5% PSG) to reach 100% confluence at 37°C and 5% CO_2. Cells were then starved of serum for 24h prior to particle exposure. The cells were exposed to AgNWs, 25μg/ml in RPMI serum free medium for 1 h pulse treatment then washed, cultured for a further hour in RPMI, washed and cultured for up to 24 h in DCCM-1 medium. After the exposure the cells were rinsed with PBS and the cells were incubated with medium containing MTS reagent according to the manufacture'sr protocol for 1.5h (CellTiter 96® AQueous One Solution Assay, Promega, USA). The absorbance of formazan product in the culture medium was then read using a plate reader at the wavelength of 490nm. Significant differences between treated and untreated TT1 cell responses were determined using unpaired *t* tests; a p value <0.05 was considered significant.

Intracellular ROS production

Intracellular oxidative stress in AgNW-exposed TT1 cells was detected by imaging the fluorescence probes resulting from oxidation of dihydroethidium (DHE). DHE is a readily permeable fluorescent dye which can be oxidized by reactive oxygen species (ROS), primarily superoxide, to yield ethidium molecules. Ethidium subsequently binds to DNA, which produces a detectable red fluorescence signal. Briefly, TT1 cells were cultured and plated on 12-well plates and exposed to AgNWs as described above. Post-exposure, cells were washed twice with warm PBS and incubated with 100 μl of 10 μM DHE (Invitrogen, Paisley UK) in culture medium for 20 minutes. At the end of DHE incubation, cells were washed twice to remove extracellular probe and preparations were visualized under inverted fluorescent microscope.

Scanning electron microscopy

The morphology and size distribution of the AgNWs were characterized using a LEO 1525 Field Emission Gun Scanning Electron Microscope (FEG-SEM). The SEM was operated in secondary electron mode at an accelerating voltage of 5 kV and the InLens detector was used. The size distribution of the AgNWs was characterized using SEM images and ImageJ software.

Transmission electron microscopy

Following the incubations, cells were rinsed briefly in saline (0.9 % NaCl) to remove any non-ingested particles and were then fixed in 2.5 % glutaraldehyde in 0.1 M PIPES buffer, pH 7.2 for 1 h at 4 °C. The fixatives were then removed by washing cells with 0.1 M PIPES buffer for 3 times. Cells were scraped and transferred into 1.5 mL Eppendorf tubes and cell pellets were obtained by centrifugation at 10,000 g for 20 min. Samples were embedded without bulk staining with osmium tetroxide. They were dehydrated in a graded ethanol series of 50%, 70%, 95%, and 100% (volume ratio of ethanol to DI-H_2O) ethanol for 5 min each then rinsed three times in acetronitrile (Sigma) for an additional 10 min each, all at room temperature. After dehydration, samples were progressively infiltrated with a Quetol-based resin, created by combining 8.75 g quetol, 13.75 g nonenyl succinic anhydride, 2.5 g methyl acid anhydride, and 0.62 g benzyl dimethylamine (all from Agar Scientific). Samples were infiltrated in 50 % resin/acetonitrile solution (volume ratio of resin to acetonitrile) for 2 h, followed by infiltration in a 75 % resin/acetonitrile solution overnight and finally in 100 % resin for 4 days with fresh resin replaced daily. Embedded samples were cureded at 60 °C for 24 h. Thin sections (70 nm) were cut directly into a water bath using an ultramicrotome with a diamond knife with a wedge an angle of 35°. Sections were immediately collected on bare, 300 mesh copper TEM grids (Agar Scientific), dried and kept under vacuum for TEM analysis.

Bright-field TEM imaging was performed on a JEOL 2000 microscope operated at 80 kV. For Figure 2 sections were post-stained with uranyl acetate and lead citrate for 5 min each before imaging. This enhances the contrast of cell structures. Extra care should be taken when handling uranium compounds (toxic and radioactive) and lead compounds (toxic).

Multiple cells (> 100 per sample) from three exposures from cells from culture were viewed in an FEI Titan 80–300 scanning/transmission electron microscope (S/TEM) operated at 80 kV, fitted with Cs (image) corrector and SiLi EDX spectrometer (EDAX, Leicester UK). HRTEM and STEM-HAADF/EDX analyses were carried out on non-stained samples (Figure 3). Over 100 intracellular AgNWs were analyzed for each cell exposure. STEM experiments were performed with a convergence semi-angle of 14 mrad and inner and outer HAADF collection angles of 49 and 239 mrad, respectively. The probe diameter was <0.5 nm. The integrated S(K)/Ag(L) peak ratio was quantified using TEM Imaging & Analysis software (FEI company, version 3.2). SAED was carried out using a camera length of 300 mm and 130–550 nm SA aperture sizes. The SAED patterns were analyzed using the DiffTools (version 3.7) which plugin for DigitalMicrograph™.[44]

Zeta Potential

The zeta potential of AgNWs in DI-H_2O was characterized by a Zetasizer Nano (Malvern Instruments Ltd, UK).

Supplementary Material

Refer to Web version on PubMed Central for supplementary material.

Acknowledgements

This work was funded in part by a grant from the NIEHS (grant number U19ES019536) and the US EPA/NERC (EPA STAR RD83469301 and NERC). AP acknowledges an ERC starting grant (Project number 257182) for additional support for AEG and SC and for support with the electron microscopy characterisation. PR acknowledges the support of a Leverhulme Trust Grant (F/07 058/BT). We thank Mr. Henock Solomon of USC for his administrative assistance.

References

1. Hillery, AM.; LIoyd, AW.; Swarbrick, J. Drug Delivery and Targeting for Pharmacists and Pharmaceutical Scientist. London: Taylor & Francis; 2001.
2. Foldbjerg R, Dang DA, Autrup H. Archives of Toxicology. 2011; 85:743–750. [PubMed: 20428844]
3. Park M, Neigh AM, Vermeulen JP, de la Fonteyne LJJ, Verharen HW, Briede JJ, van Loveren H, de Jong WH. Biomaterials. 2011; 32:9810–9817. [PubMed: 21944826]
4. Costa C, Ronconi JVV, Daufenbach JF, Goncalves CL, Rezin GT, Streck EL, Paula MMD. Mol Cell Biochem. 2010; 342:51–56. [PubMed: 20411305]
5. Suresh AK, Pelletier DA, Wang W, Morrell-Falvey JL, Gu BH, Doktycz MJ. Langmuir. 2012; 28:2727–2735. [PubMed: 22216981]
6. Kim HR, Kim MJ, Lee SY, Oh SM, Chung KH. Mutation Research-Genetic Toxicology and Environmental Mutagenesis. 2011; 726:129–135. [PubMed: 21945414]
7. Stoehr LC, Gonzalez E, Stampfl A, Casals E, Duschl A, Puntes V, Oostingh GJ. Particle and Fibre Toxicology. 2011; 8:36. [PubMed: 22208550]
8. Arora S, Jain J, Rajwade JM, Paknikar KM. Toxicology Letters. 2008; 179:93–100. [PubMed: 18508209]
9. Kang K, Jung H, Lim JS. Biomolecules & Therapeutics. 2012; 20:399–405. [PubMed: 24009827]
10. Piao MJ, Kang KA, Lee IK, Kim HS, Kim S, Choi JY, Choi J, Hyun JW. Toxicology Letters. 2011; 201:92–100. [PubMed: 21182908]
11. AshaRani PV, Mun GLK, Hande MP, Valiyaveettil S. Acs Nano. 2009; 3:279–290. [PubMed: 19236062]
12. Perry MM, Hui CK, Whiteman M, Wood ME, Adcock I, Kirkham P, Michaeloudes C, Chung KF. Am J Respir Cell Mol Biol. 2011; 45:746–752. [PubMed: 21297080]
13. Xiu ZM, Zhang QB, Puppala HL, Colvin VL, Alvarez PJJ. Nano Lett. 2012; 12:4271–4275. [PubMed: 22765771]
14. Marambio-Jones C, Hoek EMV. J Nanopart Res. 2010; 12:1531–1551.
15. Chen X, Schluesener HJ. Toxicology Letters. 2008; 176:1–12. [PubMed: 18022772]
16. Nowack B, Krug HF, Height M. Environ Sci Technol. 2011; 45:1177–1183. [PubMed: 21218770]
17. Yang X, Gondikas AP, Marinakos SM, Auffan M, Liu J, Hsu-Kim H, Meyer JN. Environmental science & technology. 2012; 46:1119–1127. [PubMed: 22148238]
18. Navarro E. Environ. Sci. Technol. 2008; 42:8959–8964. [PubMed: 19192825]
19. Choi O, Hu Z. Environmental science & technology. 2008; 42:4583–4588. [PubMed: 18605590]
20. Fabrega J, Fawcett SR, Renshaw JC, Lead JR. Environmental science & technology. 2009; 43:7285–7290. [PubMed: 19848135]

21. Yin L, Cheng Y, Espinasse B, Colman BP, Auffan M, Wiesner M, Rose J, Liu J, Bernhardt ES. Environmental science & technology. 2011; 45:2360–2367. [PubMed: 21341685]
22. Kim B, Park CS, Murayama M, Hochella MF. Environ Sci Technol. 2010; 44:7509–7514. [PubMed: 20839838]
23. Nowack B. Science. 2010; 330:1054–1055. [PubMed: 21097924]
24. Liu JY, Pennell KG, Hurt RH. Environ Sci Technol. 2011; 45:7345–7353. [PubMed: 21770469]
25. Levard C, Reinsch BC, Michel FM, Oumahi C, Lowry GV, Brown GE. Environ Sci Technol. 2011; 45:5260–5266. [PubMed: 21598969]
26. Levard C, Hotze EM, Lowry GV, Brown GE. Environ Sci Technol. 2012; 46:6900–6914. [PubMed: 22339502]
27. Reinsch BC, Levard C, Li Z, Ma R, Wise A, Gregory KB, Brown GE, Lowry GV. Environ Sci Technol. 2012; 46:6992–7000. [PubMed: 22296331]
28. Furne J, Saeed A, Levitt MD. American Journal of Physiology-Regulatory Integrative and Comparative Physiology. 2008; 295:R1479–R1485.
29. Li L, Rose P, Moore PK. Annual Review of Pharmacology and Toxicology, Vol 51, 2011. 2011; 51:169–187.
30. Donaldson K, Murphy F, Schinwald A, Duffin R, Poland CA. Nanomedicine-Uk. 2011; 6:143–156.
31. Schinwald A, Donaldson K. Part Fibre Toxicol. 2012; 9:34. [PubMed: 22929371]
32. Kemp SJ, Thorley AJ, Gorelik J, Seckl MJ, O'Hare MJ, Arcaro A, Korchev Y, Goldstraw P, Tetley TD. Am J Respir Cell Mol Biol. 2008; 39:591–597. [PubMed: 18539954]
33. Wiley B, Herricks T, Sun YG, Xia YN. Nano Lett. 2004; 4:2057–2057.
34. Beer C, Foldbjerg R, Hayashi Y, Sutherland DS, Autrup H. Toxicology Letters. 2012; 208:286–292. [PubMed: 22101214]
35. Al-Jamal KT, Nerl H, Muller KH, Ali-Boucetta H, Li SP, Haynes PD, Jinschek JR, Prato M, Bianco A, Kostarelos K, Porter AE. Nanoscale. 2011; 3:2627–2635. [PubMed: 21603701]
36. Jiang P, Zhu CN, Zhang ZL, Tian ZQ, Pang DW. Biomaterials. 2012; 33:5130–5135. [PubMed: 22484042]
37. Jiang P, Tian ZQ, Zhu CN, Zhang ZL, Pang DW. Chemistry of Materials. 2012; 24:3–5.
38. Donaldson K, Poland CA, Murphy FA, MacFarlane M, Chernova T, Schinwald A. Advanced Drug Delivery Reviews.
39. Thorley AJ, Tetley TD. Pharmacology & Therapeutics.
40. Mossman BT, Churg A. American journal of respiratory and critical care medicine. 1998; 157:1666–1680. [PubMed: 9603153]
41. Schinwald A, Chernova T, Donaldson K. Part Fibre Toxicol. 2012; 9:47. [PubMed: 23199075]
42. Maynard RL, Donaldson K, Tetley TD. Nanotoxicology. 2013; 7:350–351. [PubMed: 22292454]
43. Shimada A, Kawamura N, Okajima M, Kaewamatawong T, Inoue H, Morita T. Toxicol Pathol. 2006; 34:949–957. [PubMed: 17178695]
44. Mitchell DRG. Microscopy Research and Technique. 2008; 71:588–593. [PubMed: 18567012]

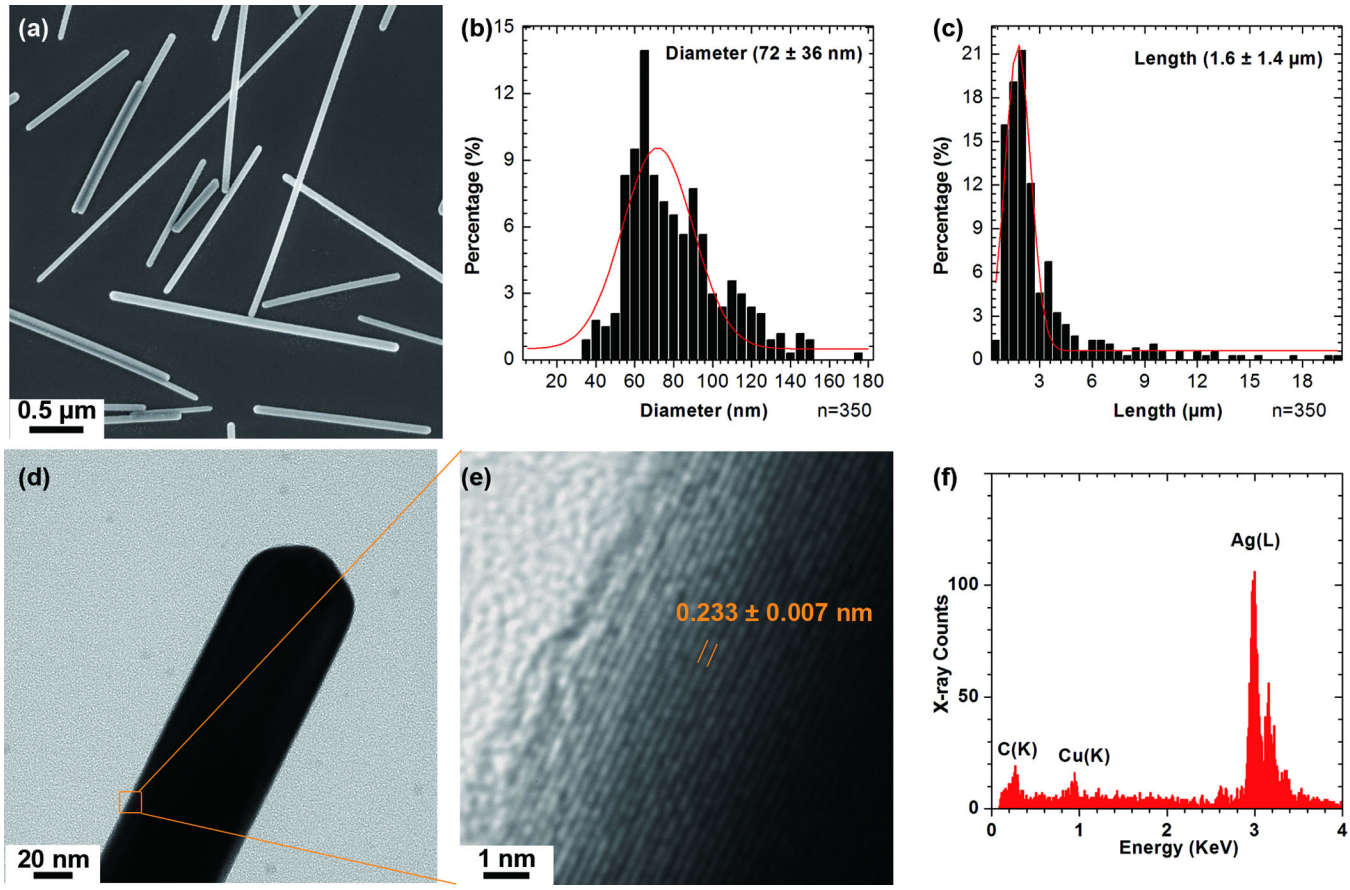

Figure1.

Characterization of the as-synthesized AgNWs. SEM image (a) of as-synthesized AgNWs, and their diameter (b) and length (c) distributions with the Gaussian fits. A BF-TEM image (d) and the corresponding HRTEM image (e) of the boxed area in (d), showing a lattice spacing of 0.24 nm. (f) A representative EDX spectrum taken from as-synthesized AgNWs.

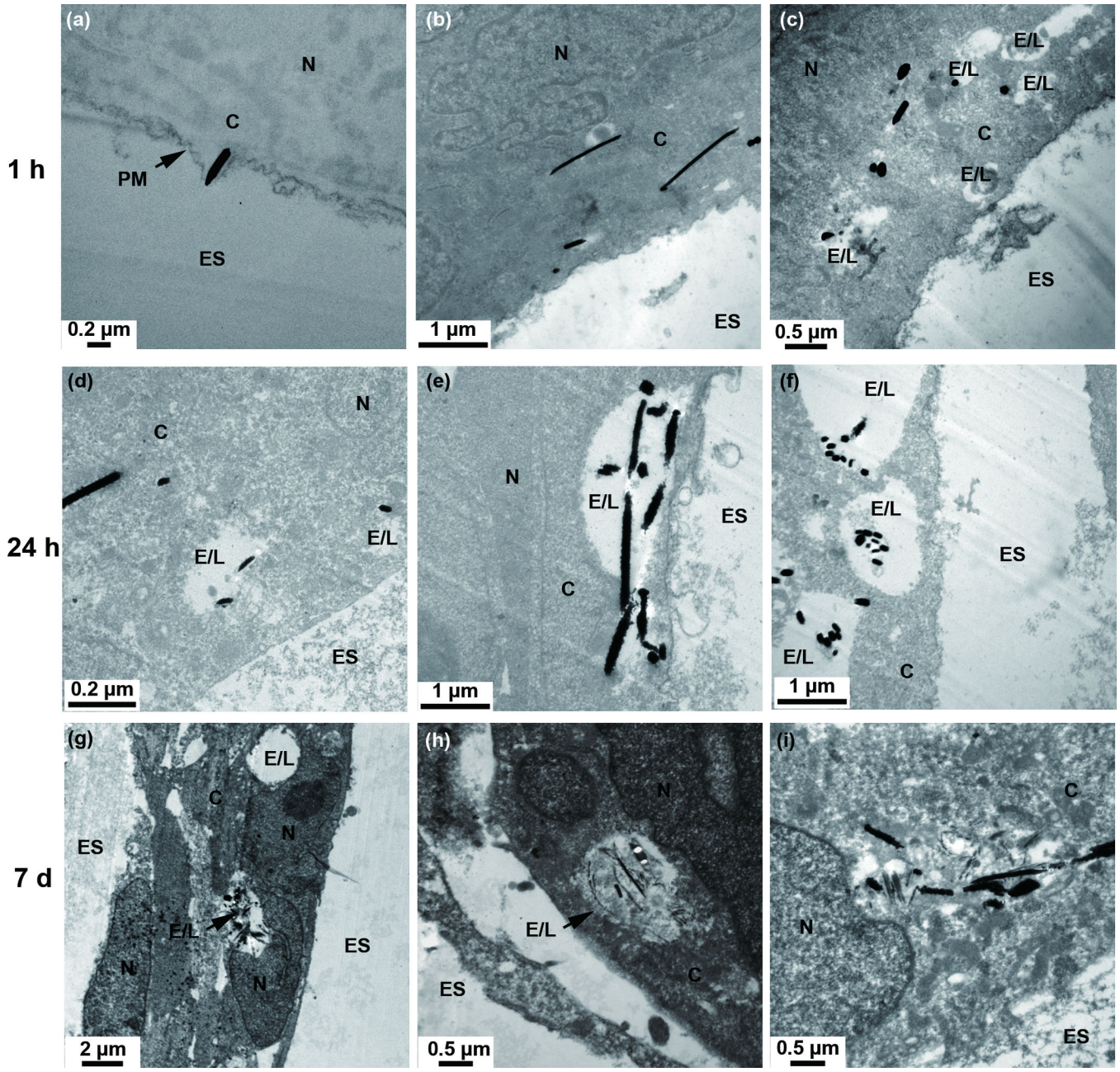

Figure 2.

TEM images showing the cellular distribution of AgNWs in TT1 epithelial cells after 1 h (a-c), 24 h (d-f) and 7 days (g-i) exposure ES = extracellular space; C = cytoplasm; E/L: endosome/lysosome; N = nucleus; PM = plasma membrane. Images (b-i) are TEM sections post-stained with uranyl acetate and lead citrate.

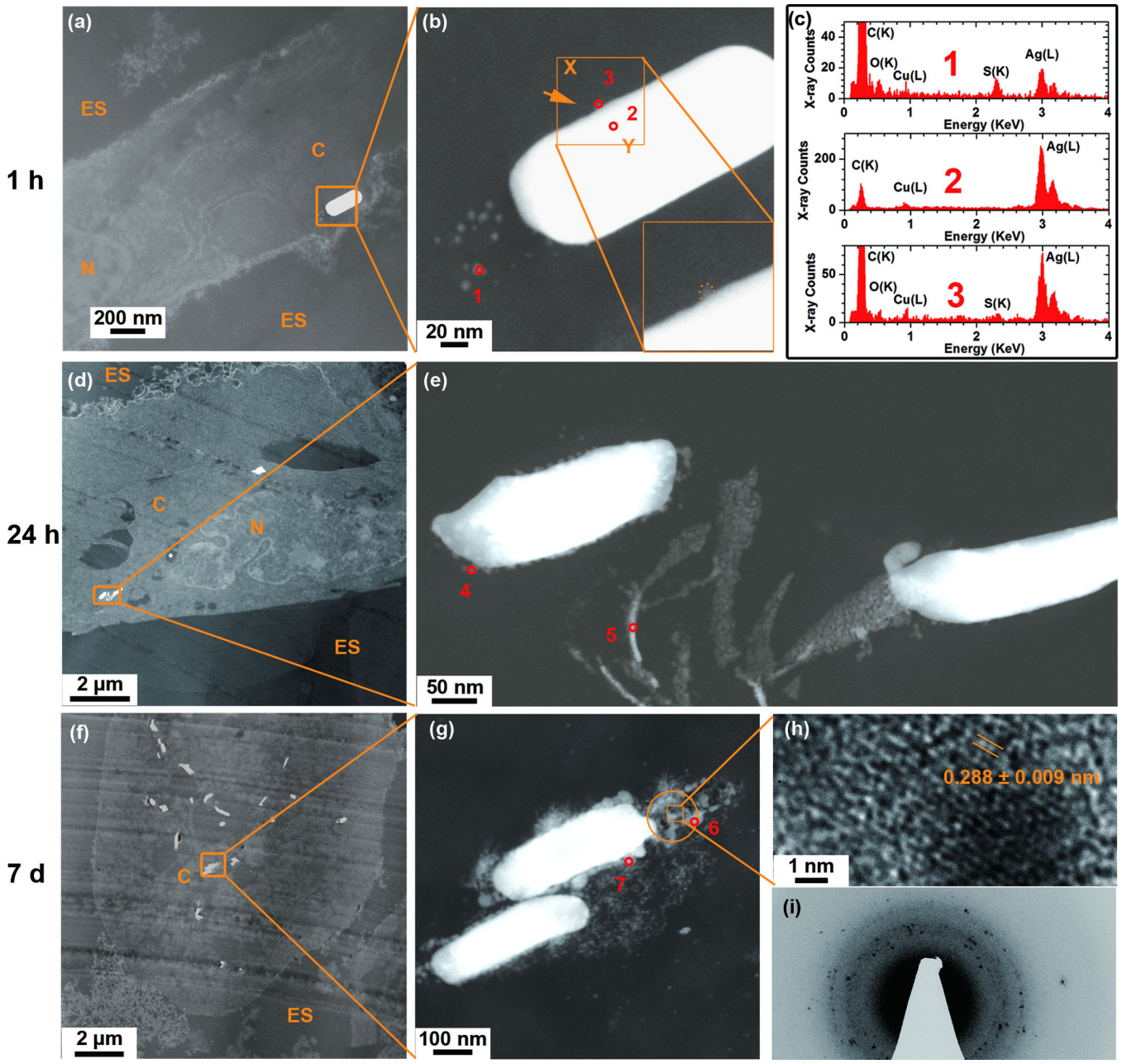

Figure 3.

Changes in the morphology and composition of the AgNWs as a function of time after their uptake by TT1 epithelial cells at 1 h (a-c), and at 24 h (d-e) and 7 days (f-i) following the pulsed exposure, using unstained cell sections. (a) HAADF-STEM image of an AgNW inside the cell cytoplasm showing particles surrounding the tip of the AgNW. (b) A corresponding higher resolution HAADF-STEM image depicts the boxed area in (a). The insert in (b) shows a higher magnification image of the AgNW edge. (c) STEM-EDX spectra taken from corresponding areas 1–3 marked in (b). (d-e) HAADF-STEM images where image (e) depicts the boxed area in (d). (f-i) HAADF-STEM images where (g) depicts the boxed area in (f). (h) An HRTEM image of the boxed area in image (g). (i) SAED

pattern from the circled area in (g) using a selected area aperture size of ~130 nm. STEM-EDX spectra collected from areas 4–7 marked in (e) and (g) are presented in supplementary, Figure S2.

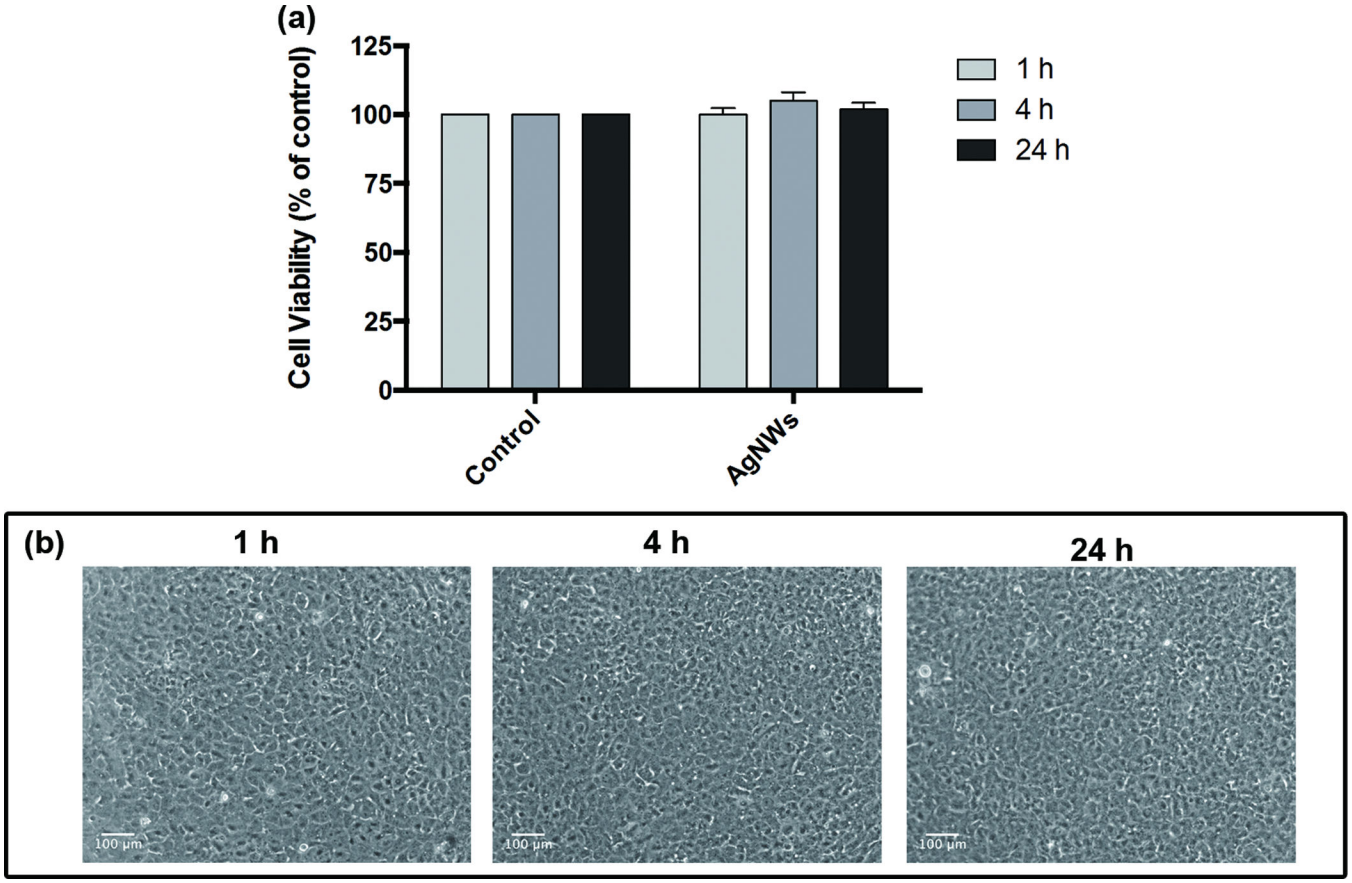

Figure 4.

TT1 cell cytotoxicity and reactive oxygen species (ROS) generation following pulse treatment with AgNWs (25 μg/ml) for one hour and cultured up to 24 h are shown in: (a) Cell viability of TT1 cells (MTS assay); the data are presented as a % of the untreated control (n=3) ± SEM; *$p < 0.05$, **$p < 0.01$. and (b) Light micrographs comprising the time-course imaging of the oxidative stress marker DHE (red) in TT1 cells, which was negative.

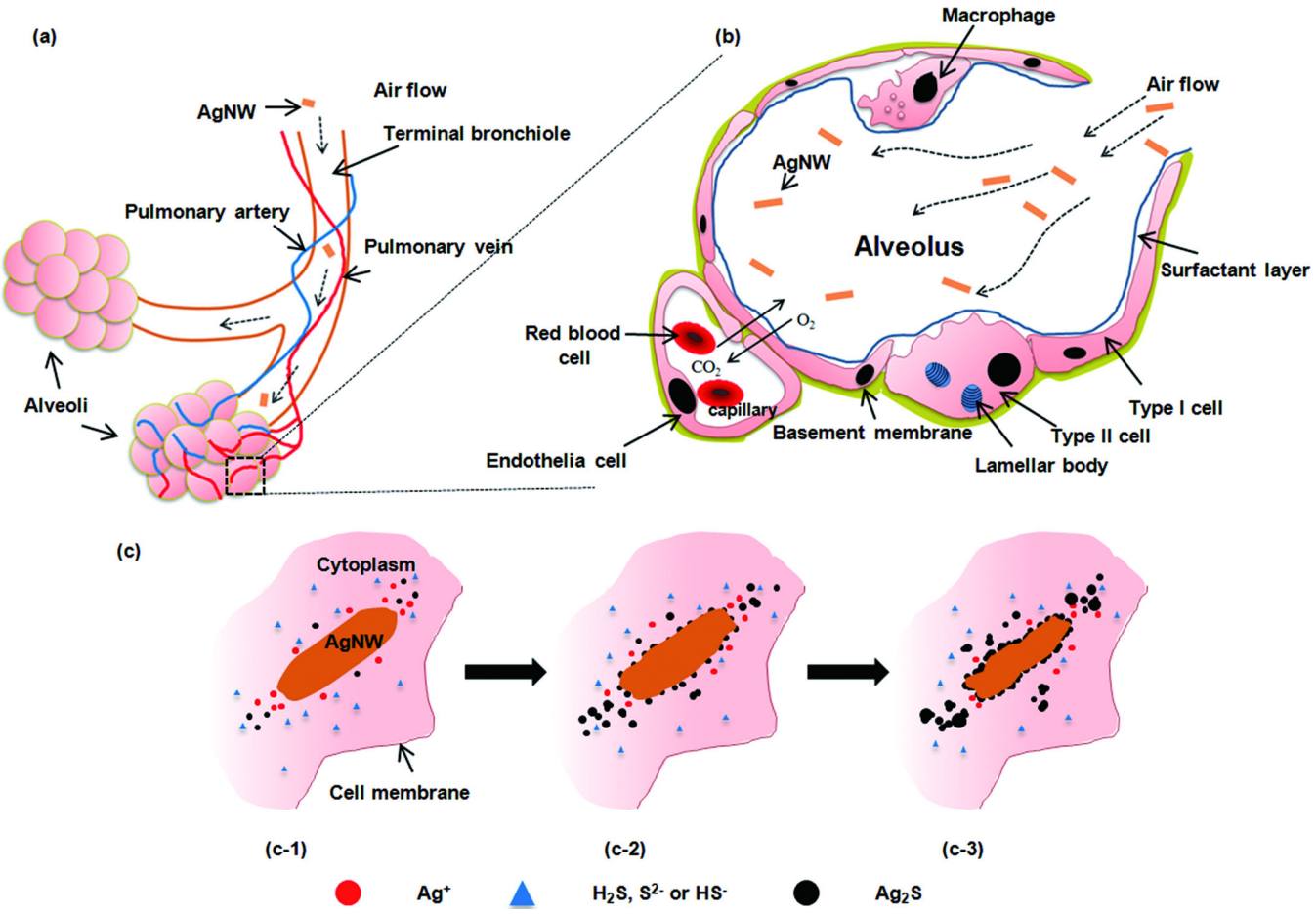

Figure 5.

(a) A schematic drawing of inhaled particles depositing into the pulmonary alveolar region, comprising the respiratory bronchioles, alveolar ducts and alveoli. Abundant pulmonary capillaries run through the alveoli to allow air-blood exchange. (b) A diagram of the cross section of one of the alveolus in the boxed area (a). The alveolar epithelium consists of type I, type II epithelial cells and alveolar macrophages, which are covered with a surfactant layer produced by type II cells. Gas exchange takes place at the epithelial-endothelial gas-blood barrier consisting of a mixed monolayer of type I and type II cells which share a basement membrane with the underlying capillary endothelium. (c) A schematic representation of the proposed sulfidation mechanism over time of AgNW inside type I epithelial cell.

Table 1

The integrated S(K)/Ag(L) peak ratio extracted from EDX spectra collected from positions 1–7 (Figure 3) after 1 h AgNW exposure, and 24 h and 7 day post-exposure.

Position	Incubation time	Description	S(K)/Ag(L) peak ratio
1	1 h	particles	0.75 ± 0.34
2	1 h	NW bulk	no S detected
3	1 h	particles on NW surface	0.12 ± 0.03
4	24 h	particles on NW surface	0.41 ± 0.13
5	24 h	clusters	1.15 ± 0.40
6	7 d	particles	0.50 ± 0.19
7	7 d	particles on NW surface	0.26 ± 0.09
In house prepared Ag_2S NPs (crystal structure confirmed by SAED)			0.44 ± 0.09